A three-dimensional multidimensional gas-kinetic scheme for the Navier–Stokes equations under gravitational fields

C.T. Tian [a], K. Xu [b,*], K.L. Chan [b], L.C. Deng [a]

[a] *National Astronomical Observatories, Chinese Academy of Sciences, Beijing, China*
[b] *Department of Mathematics, Hong Kong University of Science and Technology, Hong Kong, China*

Abstract

This paper extends the gas-kinetic scheme for one-dimensional inviscid shallow water equations (K. Xu, A well-balanced gas-kinetic scheme for the shallow-water equations with source terms, J. Comput. Phys. 178 (2002) 533–562) to multidimensional gas dynamic equations under gravitational fields. Four important issues in the construction of a well-balanced scheme for gas dynamic equations are addressed. First, the inclusion of the gravitational source term into the flux function is necessary. Second, to achieve second-order accuracy of a well-balanced scheme, the Chapman–Enskog expansion of the Boltzmann equation with the inclusion of the external force term is used. Third, to avoid artificial heating in an isolated system under a gravitational field, the source term treatment inside each cell has to be evaluated consistently with the flux evaluation at the cell interface. Fourth, the multidimensional approach with the inclusion of tangential gradients in two-dimensional and three-dimensional cases becomes important in order to maintain the accuracy of the scheme. Many numerical examples are used to validate the above issues, which include the comparison between the solutions from the current scheme and the Strang splitting method. The methodology developed in this paper can also be applied to other systems, such as semi-conductor device simulations under electric fields.
© 2007 Elsevier Inc. All rights reserved.

Keywords: Gas-kinetic scheme; Navier–Stokes equations; Gravitational field; Compressible convection

1. Introduction

Since most astrophysical problems are related to the hydrodynamical evolution in a gravitational field, the correct implementation of the gravitational force in an astrophysical hydrodynamical code is essential, especially in systems with long time integrations, such as modeling star and galaxy formation. Even though many hydrodynamical codes have been successfully applied to astrophysical problems, including the Piecewise parabolic method (PPM) and total variation diminishing (TVD) codes [5,12], most have considered only short

---

time evolutions with strong shock or expansion waves. With the slowness of galaxy evolution, many codes have difficulties due to the improper treatment of the gravitational force effect, the so-called source term in the Euler or the Navier–Stokes equations. After integration of millions of time steps, many codes cannot settle down to determine an isothermal steady state solution for a gas in a time-independent external gravitational field. The solution will either oscillate around the equilibrium solution, or simply deviate from equilibrium due to artificial heating, which triggers numerical gravitation-thermal instability, i.e., the collapse of the gas core. There have been many attempts to construct such a well-balanced gas dynamic code that preserves the hydrostatic solution accurately [8,20,2].

In recent years, the study of flow equations with source terms has attracted much attention in the computational fluid dynamics community [18]. Flow equations with source terms in one-dimensional (1D) case can be written as

$$W_t + F(W)_x = S, \tag{1}$$

where W is the vector of conservative flow variables with the corresponding fluxes $F(W)$. Here, S is the source, such as the gravitational force. If we integrate the above equation with respect to dx in a spatial element, j, from $x_{j-1/2}$ to $x_{j+1/2}$, and dt in a time interval from t^n to t^{n+1},

$$\int_{t^n}^{t^{n+1}} \int_{x_{j-1/2}}^{x_{j+1/2}} (W_t + F(W)_x) dx\, dt = \int_{t^n}^{t^{n+1}} \int_{x_{j-1/2}}^{x_{j+1/2}} S(W) dx\, dt,$$

we get

$$W_j^{n+1} - W_j^n = \frac{1}{\Delta x} \int_{t^n}^{t^{n+1}} (F_{j-1/2}(t) - F_{j+1/2}(t)) dt + \frac{1}{\Delta x} \int_{x_{j-1/2}}^{x_{j+1/2}} \int_{t^n}^{t^{n+1}} S(W) dx\, dt,$$

where $\Delta x = x_{j+1/2} - x_{j-1/2}$ is the cell size and W_j is the averaged value of W in cell j, i.e.,

$$W_j = \frac{1}{\Delta x} \int_{x_{j-1/2}}^{x_{j+1/2}} W\, dx.$$

The above equation is an integral form of Eq. (1) and is exact and equivalent to Eq. (1). In an earlier paper on the shallow water equations [16], we emphasized the importance of including the source term effect into the flux function at a cell interface in order to develop a well-balanced scheme. However, the exact equilibrium solution, such as $u = 0$ and $h + B = $ constant, for the shallow water equations, is relatively simple and special. The simplicity can be realized through the relation $dh/dx = -dB/dx = $ constant inside each computational cell once the bottom topology is approximated as a linear function inside each cell. Therefore, the MUSCL-type scheme with a single slope inside each cell can be precisely used to reconstruct the initial well-balanced solution. However, these techniques developed for the shallow water equations cannot be directly extended to gas dynamics equations. For example, the hydrostatic equilibrium solution for the gas dynamic equations may become $\rho \sim e^{-\alpha x}$, which is an exponential function. This exact equilibrium solution cannot even be precisely reconstructed as an initial condition in the MUSCL-type scheme with a single limited slope inside each numerical cell. Even though, it seems impossible to develop a well-balanced scheme for the gas dynamic equations with an error up to the order of machine zero, a proper numerical treatment is still essential to get accurate solutions.

For a gas flow under an external time-independent gravitational field, there exists an isothermal solution, the so-called hydrostatic or well-balanced equilibrium solution, with a constant temperature and zero fluid velocity. This solution is an intrinsic solution due to the balance between the flux gradient and source term, i.e., $F(W)_x = S$. However, based on the macroscopic equations, it is unclear how the gas settles down to an isothermal solution. Usually, additional assumptions, such as a constant temperature, are needed before deriving such an equilibrium result. Numerically, it is challenging to obtain such a solution. If Eq. (1) is solved by a simple operator splitting method, such as $W_t + F_x = 0$ for the flux at a cell interface and $W_t = S$ to account for the source term inside each cell, as observed frequently, many schemes simply deviate their solutions from exact ones after millions of time step integrations. The systematic errors will accumulate and eventually crash the calculation. This happens to be the so-called *numerical heating* phenomenon, which was reported in [13].

Due to the accumulation of numerical errors, the internal energy in an isolated gas system with adiabatic boundary conditions under a constant gravitational field will increase forever. Fig. 1 shows such a solution, where the internal energy goes up after millions of time steps. The non-conservation of the total energy in the system is not surprising because the gas dynamic equation (1) itself is not written in a conservative form. The problem in the gas dynamic equations is that the numerical error accumulates in one direction. On the contrary, there is no such problem in the shallow water equations even if the numerical scheme is not a well-balanced one.

Based on the Boltzmann equation, a flow under a gravitational field in a hydrostatic state can be described as

$$\vec{c} \cdot \frac{\partial f}{\partial \vec{x}} - \frac{\partial \phi}{\partial \vec{x}} \cdot \frac{\partial f}{\partial \vec{c}} = 0,$$

where f is the gas distribution function, $\vec{c}$ is the particle velocity, and ϕ is the external gravitational potential. The general solution of the above differential equation is

$$f(\vec{x}, \vec{c}) = \mathcal{F}\left(\phi + \frac{1}{2}c^2\right),$$

where $\mathcal{F}$ is an arbitrary function of $c^2 = \vec{c} \cdot \vec{c} = c_1^2 + c_2^2 + c_3^2$. This equilibrium solution clearly shows that the gas will have the same temperature, because the temperature becomes a constant multiplier for the function $\phi + \frac{1}{2}c^2$. For example, the function $\mathcal{F}$ in hydrostatic equilibrium will become $\exp\left(-\left(\frac{1}{2}c^2 + \phi\right)/RT\right)$, where RT is a constant temperature. The above analysis shows the usefulness of using a kinetic equation instead of macroscopic equations to describe a gas flow under a gravitational field. It also implicitly demonstrates that the flux functions, which are the moments of f, have to take into account the source term effect, i.e., ϕ, in the solution of f.

In the past several years, a gas-kinetic BGK Navier–Stokes (BGK-NS) scheme has been developed for compressible Navier–Stokes equations [15,9,10]. It achieves success in computing viscous flow solutions, such as the hypersonic viscous and heat conducting flows [14]. Due to the simplicity of particle transport, a multidimensional scheme can be constructed by incorporating a multidimensional particle propagation mechanism through the cell interface, where the particle transport in both normal and tangential directions of a cell interface can be taken into account. However, constructing a well-balanced BGK-NS method for gas dynamic equations under a gravitational field is not straightforward. As shown above, with a hydrostatic state, the density inside each numerical cell is distributed exponentially in space, which cannot be precisely reconstructed by
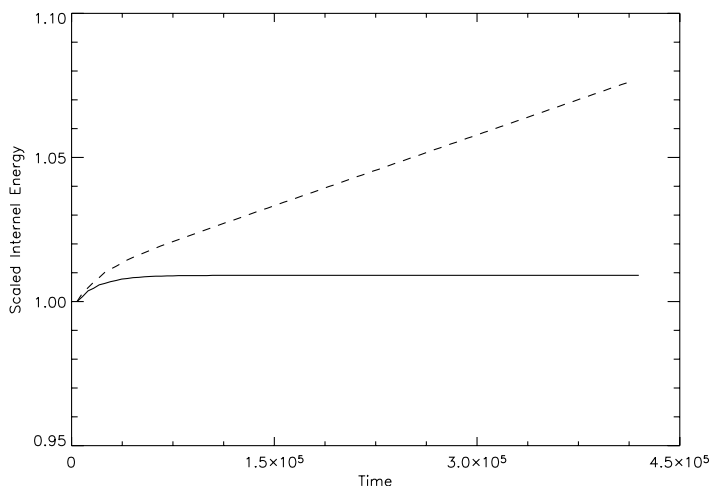

Fig. 1. Numerical heating. The time evolution of the total internal energy of an isolated system. Both solutions are computed by the BGK scheme but with different source term treatment. The total internal energy is scaled by the initial value. The dashed line is the solution from the BGK scheme without including the source term effect in the flux function and the solid line is the solution with the source term effect included in the flux.

a simple limited slope in a standard MUSCL-type scheme. In other words, even starting from the initial condition, some numerical error is already introduced. Another important issue that needs to be addressed is the Chapman–Enskog expansion of the Boltzmann equation, where the external force effect has to be added to account for the balance between the dissipative and external forcing terms. This is important to capturing the viscous flow solution, especially with a scheme that should work under both continuous and discontinuous flow conditions. To achieve a well-balanced scheme, the gravitational force effect on the particle acceleration and on the numerical flux at the cell interface needs to be explicitly taken into account as well. In order to avoid the numerical heating (cooling) effect, a consistent treatment between the source term inside each cell and the flux at the cell interface is required. The BGK scheme presented in this paper is a well-balanced scheme up to second-order accuracy. On the contrary to the shallow water solutions, the hydrostatic equilibrium state for the gas dynamic equations, such as zero flow velocity, cannot be precisely kept by the current scheme up to the machine zero, i.e., 10^{-15}. How to extend a well-balanced strategy from the shallow water equations to the gas dynamic equations remains an open problem.

This paper is organized as follows. Section 2 gives the details of the multidimensional BGK-NS scheme under a gravitational field. Section 3 presents the results from many test cases, which confirm the importance of some strategies in the development of a well-balanced scheme. At the same time, the numerical heating phenomenon is presented. The functions from the nonlinear limiter and the multidimensional transport mechanism on the well-balanced scheme are described. The last section is the conclusion.

2. BGK scheme in three-dimensional space

In this section, the multidimensional finite volume gas-kinetic scheme based on the Bhatnagar–Groos–Krook (BGK) model for the compressible Navier–Stokes equations [15] is extended to solve a flow system under an external gravitational force. The governing equations solved by the gas-kinetic scheme are written as,

$$\frac{\partial}{\partial t} \int_{\Omega} \vec{U} \, d\Omega + \oint_{\vec{S}} \vec{F} \cdot d\vec{S} = \int_{\Omega} \vec{Q} \, d\Omega, \tag{2}$$

where Ω is the control volume, $\vec{S}$ is the surface of this volume with its surface normal vector pointing outward. The macroscopic variables are

$$\vec{U}(\vec{x}, t) = (\rho, \rho\vec{u}, E)^{\mathrm{T}},$$

where ρ is the density, $\vec{u}$ is the velocity, and E is the sum of the thermal and kinetic energy. The fluxes take the form,

$$\vec{F}(\vec{x}, t) = \begin{pmatrix} \rho\vec{u} \\ \rho\vec{u} \otimes \vec{u} + p\overline{\overline{I}} - \overline{\overline{\Sigma}} \\ (E + p)\vec{u} - \kappa\nabla T - \overline{\overline{\Sigma}} \cdot \vec{u} \end{pmatrix},$$

where $\otimes$ denotes the tensor product of the vectors, κ is the thermal conductivity coefficient, $\overline{\overline{I}}$ is the unit tensor, and $\overline{\overline{\Sigma}}$ stands for the viscous shear stress tensor,

$$\Sigma_{ij} = \mu(\partial_i u_j + \partial_j u_i) - \varsigma(\nabla \cdot \vec{u})\delta_{ij},$$

where μ and ς are the first and second viscosity coefficients. The source terms can be written as follows:

$$\vec{Q} = (0, -\rho\nabla\phi, -\rho\vec{u} \cdot \nabla\phi)^{\mathrm{T}},$$

where $\phi = \phi(\vec{x}, t)$ is the gravitational potential.

The BGK scheme is a finite volume method. In Cartesian coordinates, Eq. (2) is discretized as

$$\vec{U}_j^{n+1} = \vec{U}_j^n - \frac{1}{x_{j+1/2} - x_{j-1/2}} \int_{t^n}^{t^{n+1}} (\vec{F}_{j+1/2}(t) - \vec{F}_{j-1/2}(t)) dt + \int_{t^n}^{t^{n+1}} \vec{Q}_j \, dt, \tag{3}$$

where $\vec{U}_j$ and $\vec{Q}_j$ represent the cell-averaged quantities in the jth cell, and $\vec{F}_{j+1/2}(t)$ is the vector of time-dependent fluxes across the cell interface between the jth and $j + 1$th cells.

Generally, there are three stages in a shock capturing finite volume scheme, i.e., reconstruction of initial data, gas evolution, and projection. In the reconstruction stage, a piecewise continuous flow distribution inside each cell is obtained. Then, in the gas evolution stage, a time-dependent flux, $\vec{F}_{j+1/2}(t)$, is computed based on the local solution at the cell interface, such as the solution of a Riemann problem. Based on the fluxes, the cell average flow quantities can be updated to a new time level. At the same time, the source term contribution has to be added on the time evolution of the flow variables inside each cell.

2.1. Reconstruction

In the higher-order finite volume method, the cell-averaged flow variables have to be reconstructed first to obtain the quantities at the cell boundaries. The reconstruction depends solely on the flow distribution at the beginning of each time step. In the smooth flow region, a direct connection of cell averages across a cell interface is a good choice,

$$\vec{U}_{j+1/2} = \frac{\vec{U}_{j+1} + \vec{U}_j}{2}, \tag{4}$$

where $\vec{U}_{j+1/2}$ stands for the flow variables at the interface, and the slope across the cell interface becomes $(\vec{U}_{j+1} - \vec{U}_j)/(x_{j+1} - x_j)$. A higher-order interpolation can be used to improve the spatial accuracy of the scheme. In a discontinuous flow region, the *kinematic* dissipation is added implicitly to the reconstructed initial data by converting kinetic energy into thermal one [15]. The amount of *kinematic* dissipation depends on the limiters used. In the current study, the van Leer limiter is adopted. For the sake of simplicity, let $\vec{U}_{j+1}(x_{j+1/2})$ denote the reconstructed data on the right-hand side of the interface $(x_{j+1/2})$ and let $\vec{U}_j(x_{j+1/2})$ be the data on the left-hand side. Then,

$$\vec{U}_j(x_{j+1/2}) = \vec{U}_j(x_j) + (x_{j+1/2} - x_j)L_j, \tag{5}$$

$$\vec{U}_{j+1}(x_{j+1/2}) = \vec{U}_{j+1}(x_{j+1}) - (x_{j+1} - x_{j+1/2})L_{j+1}. \tag{6}$$

In the above expressions, the van Leer limiter is defined as,

$$L_j = S(s_+, s_-)\frac{|s_+||s_-|}{|s_+| + |s_-|},$$

where $S(s_+, s_-) = \text{sign}(s_+) + \text{sign}(s_-)$, $s_+ = (\vec{U}_{j+1} - \vec{U}_j)/(x_{j+1} - x_j)$, and $s_- = (\vec{U}_j - \vec{U}_{j-1})/(x_j - x_{j-1})$.

2.2. Gas evolution

In the BGK scheme, the flow evolution is governed by the BGK equation [1],

$$\frac{\partial f}{\partial t} + \vec{c} \cdot \nabla f + (-\nabla\phi) \cdot \nabla_{\vec{c}}f = \frac{g - f}{\tau}, \tag{7}$$

where $f(\vec{x}, \vec{c}, t)$ is the gas distribution function, $\vec{c}$ is the particle velocity, τ is the collision time, and $\nabla_{\vec{c}} = (\partial/\partial c_1, \partial/\partial c_2, \partial/\partial c_3)$. The right-hand side of (7) is the so-called relaxation model, which is a simplification of the collision term of the Botlzmann equation [19]. The equilibrium state, g, in Eq. (7) is a Maxwellian distribution,

$$g = \rho\left(\frac{\lambda}{\pi}\right)^{\frac{N+3}{2}} e^{-\lambda((\vec{c}-\vec{u})\cdot(\vec{c}-\vec{u})+\xi^2)},$$

where ξ has N internal degrees of freedom, such as the molecular rotation, λ is related to the gas temperature by $\lambda = m/2kT$, m is the molecular mass, k is the Boltzmann constant, and T is the temperature. The above expression is for a gas in three dimensions. For 1D and 2D flow simulations, the degree of freedom K of the variable ξ is defined as $K = N + 2$ for 1D flow and $K = N + 1$ for 2D flow, where 2 stands for the particle random motion in the x_2 and x_3 directions and 1 accounts for the x_3 direction random motion only. In a 3D

simulation, K is equal to N. In the equilibrium state, the internal energy variable, ξ^2, is defined as $\xi^2 = \xi_1^2 + \xi_2^2 + \cdots + \xi_K^2$.

The relation between the macroscopic variable, $\vec{U}$, and the distribution function, f, is

$$\vec{U} = \int_{-\infty}^{+\infty} \vec{\psi} f \, \mathrm{d}\Xi, \quad \vec{\psi} = [1, \vec{c}, \frac{1}{2}(\vec{c} \cdot \vec{c} + \xi^2)]^{\mathrm{T}},$$

where $\mathrm{d}\Xi = \mathrm{d}\vec{c}\,\mathrm{d}\xi$ is the volume element in the phase space with $\mathrm{d}\xi = \mathrm{d}\xi_1 \mathrm{d}\xi_2 \ldots \mathrm{d}\xi_K$. The moments of a Maxwellian are given in Appendix A of [15].

The Navier–Stokes equations can be regarded as a low-order approximation of the BGK equation for the linearly distributed flow variables in space with non-zero velocity and temperature gradients. It has been shown that for a monoatomic [19] and polyatomic gas [17], the Navier–Stokes equations can be derived from the BGK model with the dissipative coefficients,

$$\mu = \tau p, \quad \varsigma = \frac{2}{3}\frac{N}{N+3}\tau p, \quad \kappa = \frac{N+5}{2}\frac{k}{m}\tau p,$$

which are the dynamical viscosity coefficient, the second viscosity coefficient, and the thermal conductivity, respectively. For an ideal gas, the equation of state becomes $p = \rho/2\lambda$.

The right-hand side of Eq. (7) describes a relaxation process from an initial non-equilibrium state, f, to an equilibrium state, g, through particle collisions. Here, τ is called the particle relaxation time. Assume that τ is a local constant and integrate Eq. (7) along its particle trajectory,

$$\frac{\mathrm{d}\vec{x}'}{\mathrm{d}t'} = \vec{c}' - \nabla\phi t', \qquad \frac{\mathrm{d}\vec{c}'}{\mathrm{d}t'} = -\nabla\phi.$$

We have

$$f(\vec{x}, \vec{c}, t) = \frac{1}{\tau}\int_0^t g\,\mathrm{e}^{-(t-t')/\tau}\mathrm{d}t' + \mathrm{e}^{-t/\tau}f(\vec{x}_0, \vec{c}_0, 0), \tag{8}$$

where $0 < t' < t$ and

$$\vec{c}_0 = \vec{c} - (-\nabla\phi)t, \quad \vec{x}_0 = \vec{x} - \vec{c}t + \frac{1}{2}(-\nabla\phi)t^2$$

are respectively the particle velocity and trajectory with initial position $\vec{x}_0$ and velocity $\vec{c}_0$. The gravitational effect has been included in the particle acceleration and trajectory change. Since the term $\frac{1}{2}(-\nabla\phi)t^2$ has a third-order effect on a numerical scheme, it will be ignored in the construction of the time-dependent solution, f, in the following.

The integral of the right-hand side of Eq. (8) is generally difficult to evaluate because the equilibrium state, g, itself is implicitly related to f, and the initial distribution, $f(\vec{x}_0, \vec{c}_0, t' = 0)$, is unknown. In the BGK scheme, both are modeled as first-order expansions of a local equilibrium distribution with the inclusion of the Chapman–Enskog expansion for the dissipative term. To include the effect of gravitational force in the non-equilibrium gas distribution, the initial distribution, $f_0 = f(\vec{x}_0, \vec{c}_0, t' = 0)$, is further developed as

$$f_0 = \begin{cases} g_0^{\mathrm{l}}[1 - \vec{a}^{\mathrm{l}} \cdot \vec{c}t - \vec{b}^{\mathrm{l}} \cdot (-\nabla\phi)t - \tau(\vec{a}^{\mathrm{l}} \cdot \vec{c} + \vec{b}^{\mathrm{l}} \cdot (-\nabla\phi) + A^{\mathrm{l}})], & x \leqslant 0 \\ g_0^{\mathrm{r}}[1 - \vec{a}^{\mathrm{r}} \cdot \vec{c}t - \vec{b}^{\mathrm{r}} \cdot (-\nabla\phi)t - \tau(\vec{a}^{\mathrm{r}} \cdot \vec{c} + \vec{b}^{\mathrm{r}} \cdot (-\nabla\phi) + A^{\mathrm{r}})], & x \geqslant 0, \end{cases} \tag{9}$$

where

$$g_0^{\mathrm{l}} = \rho_j(x_{j+1/2})\left(\frac{\lambda_j(x_{j+1/2})}{\pi}\right)^{\frac{N+3}{2}} \mathrm{e}^{\{-\lambda_j(x_{j+1/2})((\vec{c}-\vec{u}_j(x_{j+1/2}))\cdot(\vec{c}-\vec{u}_j(x_{j+1/2}))+\xi^2)\}}$$

and

$$g_0^{\mathrm{r}} = \rho_{j+1}(x_{j+1/2})\left(\frac{\lambda_{j+1}(x_{j+1/2})}{\pi}\right)^{\frac{N+3}{2}} \mathrm{e}^{\{-\lambda_{j+1}(x_{j+1/2})((\vec{c}-\vec{u}_{j+1}(x_{j+1/2}))\cdot(\vec{c}-\vec{u}_{j+1}(x_{j+1/2}))+\xi^2)\}}$$

are the equilibrium distributions at the left- and right-hand sides of the cell interface. The slopes in Eq. (9) are defined as $\vec{a}^{\mathrm{l}} = \nabla \ln g_0^{\mathrm{l}}$, $\vec{a}^{\mathrm{r}} = \nabla \ln g_0^{\mathrm{r}}$, $\vec{b}^{\mathrm{l}} = \nabla_{\vec{c}} \ln g_0^{\mathrm{l}}$, $\vec{b}^{\mathrm{r}} = \nabla_{\vec{c}} \ln g_0^{\mathrm{r}}$, $A^{\mathrm{l}} = \partial \ln g_0^{\mathrm{l}} / \partial t$, $A^{\mathrm{r}} = \partial \ln g_0^{\mathrm{r}} / \partial t$. The above model is an extension of the Chapman–Enskog expansion in [15], where the gravitational force term has been added in the modification of the non-equilibrium state. The term proportional to τ corresponds to the dissipative terms in the Navier–Stokes equations. The gravitational force makes two contributions on f_0. One is the particle acceleration in the transport process to a cell interface, and the other is in the non-equilibrium initial state. Note that in the above initial gas distribution function, the flow variation in the tangential direction is also included in the definition of $\vec{a}^{\mathrm{l}}$ and $\vec{a}^{\mathrm{r}}$.

All slopes in (9) can be uniquely evaluated from the reconstructed flow variables and their derivatives. In the normal direction of a cell interface, $(x_{j+1/2})$, the slopes on the left-hand side can be expressed as

$$a_j^{\mathrm{l}} = \vec{a}^{\mathrm{l}} \cdot \vec{\psi},$$

where $\vec{a}^{\mathrm{l}}$ is a local constant vector. Based on the relation between the distribution function and the macroscopic variables, we have

$$\frac{\vec{U}_j(x_{j+1/2}) - \vec{U}_j(x_j)}{x_{j+1/2} - x_j} = \int a_j^{\mathrm{l}} \vec{\psi} g_0^l \, \mathrm{d}\Xi = \vec{a}^{\mathrm{l}} \int \vec{\psi} \otimes \vec{\psi} g_0^l \, \mathrm{d}\Xi.$$

The above linear system can be solved directly for a_j^{l} and the detailed formulation is given in the appendix for the 3D case. Similarly, the slopes on the right-hand side of the interface can be obtained by solving

$$\frac{\vec{U}_{j+1}(x_{j+1}) - \vec{U}_{j+1}(x_{j+1/2})}{x_{j+1} - x_{j+1/2}} = \int a_j^{\mathrm{r}} \vec{\psi} g_0^r \, \mathrm{d}\Xi.$$

In the tangential direction (x_k) of the cell interface, the slopes are obtained from

$$\frac{\vec{U}_{j,k+1}(x_{j+1/2}) - \vec{U}_{j,k-1}(x_{j+1/2})}{x_{j+1/2,k+1} - x_{j+1/2,k-1}} = \int a_k^{\mathrm{l}} \vec{\psi} g_0^l \, \mathrm{d}\Xi,$$

$$\frac{\vec{U}_{j+1,k+1}(x_{j+1/2}) - \vec{U}_{j+1,k-1}(x_{j+1/2})}{x_{j+1/2,k+1} - x_{j+1/2,k-1}} = \int a_k^{\mathrm{r}} \vec{\psi} g_0^r \, \mathrm{d}\Xi.$$

The terms multiplied by τ in Eq. (9) represent the non-equilibrium part of a Chapman–Enskog expansion, and make no direct contribution to the conservative flow variables. Therefore, based on

$$\int (\vec{a}^{\mathrm{l}} \cdot \vec{c} + \vec{b}^{\mathrm{l}} \cdot (-\nabla\phi) + A^{\mathrm{l}}) \vec{\psi} g_0^l \, \mathrm{d}\Xi = 0,$$

$$\int (\vec{a}^{\mathrm{r}} \cdot \vec{c} + \vec{b}^{\mathrm{r}} \cdot (-\nabla\phi) + A^{\mathrm{r}}) \vec{\psi} g_0^r \, \mathrm{d}\Xi = 0,$$

the temporal slopes A^l and A^r can be determined. Note that, for the first time, the gravitational force effect on the determination of the non-equilibrium state has been proposed in the above equations.

The equilibrium state $g(\vec{x}', \vec{c}', t')$ in the integral solution is constructed by a Taylor series expansion of a local equilibrium distribution around $(\vec{x}, \vec{c}, 0)$. With the inclusion of the external source effects, it has the form

$$g = \begin{cases} g_0[1 - (t-t')\bar{a}_n^{\mathrm{l}} c_n - (t-t')\bar{b}_n^{\mathrm{l}}(-\nabla\phi)_n - (t-t')\bar{\vec{a}}_t \cdot \vec{c}_t - (t-t')\bar{\vec{b}}_t \cdot (-\nabla\phi)_t + \overline{A}t'], & c_n \leqslant 0 \\ g_0[1 - (t-t')\bar{a}_n^{\mathrm{r}} c_n - (t-t')\bar{b}_n^{\mathrm{r}}(-\nabla\phi)_n \quad - (t-t')\bar{\vec{a}}_t \cdot \vec{c}_t - (t-t')\bar{\vec{b}}_t \cdot (-\nabla\phi)_t + \overline{A}t'], & c_n \geqslant 0 \end{cases}$$

(10)

where

$$g_0 = \rho_0 \left(\frac{\lambda_0}{\pi}\right)^{\frac{N+3}{2}} \mathrm{e}^{-\lambda_0((\vec{c}-\vec{u}_0)\cdot(\vec{c}-\vec{u}_0)+\xi^2)}.$$

The parameters in (10) with subscript n represent the normal components of the vectors to the cell interface, and those with subscript t stand for the tangential components. This is again an extension of g in [15]. It will be

shown in Section 3 that the inclusion of both the external source term and the flow gradients in the tangential direction in the expressions of f_0 (9) and g (10) is very important to obtain a well-balanced scheme and to improve the accuracy and stability of the scheme.

In order to determine all parameters in g (10), the equilibrium state $(\vec{U}_0)$ at the cell interface at $t = 0$ must be obtained first. Since the f_0 is totally determined, taking the limit $t \to 0$ in Eq. (8) and substituting its solution into conservation constraint $\int (g - f)\vec{\psi} \mathrm{d}\Xi = 0$ at the cell interface, we have

$$\int g_0 \vec{\psi}\,\mathrm{d}\Xi = \vec{U}_0 = \int_{c_n>0} \int g_0^\mathrm{l} \vec{\psi}\,\mathrm{d}\Xi + \int_{c_n<0} \int g_0^\mathrm{r} \vec{\psi}\,\mathrm{d}\Xi.$$

Then, the slopes in Eq. (10) can be obtained through

$$\frac{\vec{U}_0 - \vec{U}_j(x_j)}{x_{j+1/2} - x_j} = \int \bar{a}_n^\mathrm{l} \vec{\psi} g_0\,\mathrm{d}\Xi,$$

$$\frac{\vec{U}_{j+1}(x_{j+1}) - \vec{U}_0}{x_{j+1} - x_{j+1/2}} = \int \bar{a}_n^\mathrm{r} \vec{\psi} g_0\,\mathrm{d}\Xi,$$

in the normal direction on the left- and right-hand sides of the cell interface, and

$$\int \bar{a}_t \vec{\psi}\,\mathrm{d}\Xi = \int_{c_n>0} \int a_t^\mathrm{l} g_0^\mathrm{l} \vec{\psi}\,\mathrm{d}\Xi + \int_{c_n<0} \int a_t^\mathrm{r} g_0^\mathrm{r} \vec{\psi}\,\mathrm{d}\Xi,$$

in the tangential direction.

The only unknown in the expression of g (10) is $\overline{A}$. By substituting the approximations (9) and (10) into the general solution (8), we have

$$\begin{aligned}
f = &\{(1 - \mathrm{e}^{-t/\tau}) + (\mathrm{e}^{-t/\tau}(t + \tau) - \tau)[(\bar{a}_n^\mathrm{l} c_n + \bar{b}_n^\mathrm{l}(-\nabla\phi)_n)H[c_n] + (\bar{a}_n^\mathrm{r} c_n + \bar{b}_n^\mathrm{r}(-\nabla\phi)_n)(1 - H[c_n]) \\
&+ \bar{a}_t \cdot \vec{c}_t + \bar{b}_t \cdot (-\nabla\phi)_t] + [t - \tau(1 - \mathrm{e}^{-t/\tau})]\overline{A}\}g_0 + \mathrm{e}^{-t/\tau}\{[1 - \vec{a}^\mathrm{l} \cdot \vec{c}t - \vec{b}^\mathrm{l} \cdot (-\nabla\phi)t \\
&- \tau(\vec{a}^\mathrm{l} \cdot \vec{c} + \vec{b}^\mathrm{l} \cdot (-\nabla\phi) + A^\mathrm{l})]H[c_n]g_0^\mathrm{l} + [1 - \vec{a}^\mathrm{r} \cdot \vec{c}t - \vec{b}^\mathrm{r} \cdot (-\nabla\phi)t - \tau(\vec{a}^\mathrm{r} \cdot \vec{c} + \vec{b}^\mathrm{r} \cdot (-\nabla\phi) + A^\mathrm{r})] \\
&\times (1 - H[c_n])g_0^\mathrm{r}\},
\end{aligned} \tag{11}$$

where the Heaviside function $H[x]$ is defined by

$$H[x] = \begin{cases} 0, & x < 0, \\ 1, & x \geqslant 0. \end{cases}$$

Due to the conservation of the conservative flow variables during particle collisions, the moment of the right-hand side of equation (7) should vanish. At the cell interface, the compatibility condition gives

$$\int_0^{\Delta t} \int (g - f)\vec{\psi}\,\mathrm{d}t\,\mathrm{d}\Xi = 0,$$

from which we get

$$\begin{aligned}
\gamma_0 \int \overline{A}\vec{\psi} g_0\,\mathrm{d}\Xi = &\int [\gamma_1 g_0 + \gamma_2 g_0((\bar{a}_n^\mathrm{l} c_n + \bar{b}_n^\mathrm{l}(-\nabla\phi)_n)H[c_n] + (\bar{a}_n^\mathrm{r} c_n + \bar{b}_n^\mathrm{r}(-\nabla\phi)_n)(1 - H[c_n]) \\
&+ \bar{a}_t \cdot \vec{c}_t + \bar{b}_t \cdot (-\nabla\phi)_t) + \gamma_3(H[c_n]g_0^\mathrm{l} + (1 - H[c_n])g_0^\mathrm{r}) + (\gamma_4 + \gamma_5)(H[c_n](\vec{a}^\mathrm{l} \cdot \vec{c} + \vec{b}^\mathrm{l} \cdot (-\nabla\phi))g_0^\mathrm{l} \\
&+ (1 - H[c_n])(\vec{a}^\mathrm{r} \cdot \vec{c} + \vec{b}^\mathrm{r} \cdot (-\nabla\phi))g_0^\mathrm{r}) + \gamma_5(H[c_n]A^\mathrm{l} g_0^\mathrm{l} + (1 - H[c_n])A^\mathrm{r} g_0^\mathrm{r})]\vec{\psi}\,\mathrm{d}\Xi,
\end{aligned}$$

where

$$\gamma_0 = \int \tau(1 - \mathrm{e}^{-t/\tau})\mathrm{d}t = \tau[\Delta t - \tau(1 - \mathrm{e}^{-\Delta t/\tau})],$$

$$\gamma_1 = \int \mathrm{e}^{-t/\tau}\mathrm{d}t = -\tau[\mathrm{e}^{-\Delta t/\tau} - 1],$$

$$\gamma_2 = \int -(\mathrm{e}^{-t/\tau}(t + \tau) - \tau)\mathrm{d}t = -\Delta t - (\gamma_4 + \gamma_5),$$

$$\gamma_3 = \int -\mathrm{e}^{-t/\tau}\,\mathrm{d}t = -\gamma_1,$$

$$\gamma_4 = \int t\,\mathrm{e}^{-t/\tau}\,\mathrm{d}t = -\tau[\Delta t\mathrm{e}^{-\Delta t/\tau} - \tau(1 - \mathrm{e}^{-\Delta t/\tau})],$$

$$\gamma_5 = \int \tau\,\mathrm{e}^{-t/\tau}\,\mathrm{d}t = \tau\gamma_1.$$

Therefore, $\overline{A}$ is fully determined from the above equations. As a result, the time-dependent gas distribution function, $f(\vec{x}, \vec{c}, t)$, is obtained. The corresponding fluxes in the x_j direction across the cell interface can be computed by

$$\vec{F}_{j+1/2} = (F_\rho, F_{\rho\vec{u}}, F_E)^{\mathrm{T}}_{j+1/2} = \int c_j f \vec{\psi}\,\mathrm{d}\Xi$$

$$= \int [\Gamma_1 g_0 + \Gamma_0 \overline{A} g_0 + \Gamma_2((\bar{a}^{\mathrm{l}}_n c_n + \bar{b}^{\mathrm{l}}_n(-\nabla\phi)_n)H[c_n] + (\bar{a}^{\mathrm{r}}_n c_n + \bar{b}^{\mathrm{r}}_n(-\nabla\phi)_n)(1 - H[c_n]) + \vec{\bar{a}}_t \cdot \vec{c}_t$$

$$+ \vec{\bar{b}}_t \cdot (-\nabla\phi)_t)g_0 + \Gamma_3(H[c_n]g_0^{\mathrm{l}} + (1 - H[c_n])g_0^{\mathrm{r}}) + (\Gamma_4 + \Gamma_5)(H[c_n](\vec{a}^{\mathrm{l}} \cdot \vec{c} + \vec{b}^{\mathrm{l}} \cdot (-\nabla\phi))g_0^{\mathrm{l}}$$

$$+ (1 - H[c_n])(\vec{a}^{\mathrm{r}} \cdot \vec{c} + \vec{b}^{\mathrm{r}} \cdot (-\nabla\phi))g_0^{\mathrm{r}}) + \Gamma_5(H[c_n]A^{\mathrm{l}}g_0^{\mathrm{l}} + (1 - H[c_n])A^{\mathrm{r}}g_0^{\mathrm{r}})]\vec{\psi}c_j\,\mathrm{d}\Xi, \tag{12}$$

where

$$\Gamma_0 = \frac{1}{2}\Delta t^2 - \tau\Delta t + \tau(1 - \mathrm{e}^{-\Delta t/\tau}),$$

$$\Gamma_1 = \Delta t + \tau(\mathrm{e}^{-\Delta t/\tau} - 1),$$

$$\Gamma_2 = -\tau\gamma_2,$$

$$\Gamma_3 = -\tau\gamma_3,$$

$$\Gamma_4 = -\tau\gamma_4,$$

$$\Gamma_5 = -\tau\gamma_5.$$

The above formulation is based on the discontinuous initial condition at the cell interface, and the above scheme can be faithfully applied to a flow with discontinuities. For a smooth flow, based on the reconstruction without using the limiter, the cell interface discontinuity will automatically disappear. So, under this condition, we have

$$\vec{a}^{\mathrm{l}} = \vec{a}^{\mathrm{r}} = \vec{\bar{a}}, \quad \vec{b}^{\mathrm{l}} = \vec{b}^{\mathrm{r}} = \vec{\bar{b}}, \quad A^{\mathrm{l}} = A^{\mathrm{r}} = \overline{A}.$$

Therefore, the solution of the BGK equation (8) will simply go to

$$f(\vec{x}, \vec{c}, t) = g(\vec{x}, \vec{c}, 0)[1 - \tau(\vec{\bar{a}} \cdot \vec{c} + \vec{\bar{b}} \cdot (-\nabla\phi) + \overline{A}) + \overline{A}t]. \tag{13}$$

From this solution, we can clearly see that the BGK solution from a general discontinuous initial condition will go to the well-defined continuous solution automatically, i.e., the Chapman–Enskog expansion for a smooth flow under a gravitational field. In other words, the multidimensional BGK scheme satisfies the consistency requirement. Within a time scale, τ, the particle acceleration due to the gravity will distort the distribution from the equilibrium through the term $\vec{\bar{b}} \cdot (-\nabla\phi)$.

It is well known that the BGK model has an intrinsic unit Prandtl number. To make the BGK scheme simulate any heat-conducting flow, the energy flux related to the heat conduction part in (12) can be modified [15] to

$$\vec{F}_E^{\mathrm{new}} = \vec{F}_E + (1/Pr - 1)\vec{q},$$

where $\vec{q}$ is the heat flux in the normal direction of the cell interface and Pr is the Prandtl number. According to the gas-kinetic theory, the heat flux is a result of energy transport carried by molecules in their random movement. In the x_i direction, $\vec{q}$ can be evaluated by

$$q_i = \frac{1}{2}\int (c_i - u_i)((\vec{c} - \vec{u}) \cdot (\vec{c} - \vec{u}) + \xi^2)f\,\mathrm{d}\Xi.$$

With a discontinuous initial condition, the collision time has the form [15],

$$\tau = \frac{\mu_0}{p_0} + \frac{|\rho_l/\lambda_l - \rho_r/\lambda_r|}{|\rho_l/\lambda_l + \rho_r/\lambda_r|}\Delta t,$$

where the first term comes from the Chapman–Enskog theory of the BGK model, which states that the particle collision time is related to the ratio of the dynamical viscosity coefficient to the pressure. The second term enhances the dynamical dissipation in cases of flow discontinuity. In the smooth flow region or around the slip line, the numerical dissipation introduced above is very small because of the continuous pressure distribution.

The above formulation clearly shows the complexity of the gas-kinetic scheme for the Navier–Stokes solutions under a gravitational field. The splitting of a Maxwellian distribution into two half ones leads to a very complicated flux splitting method with error functions and terms involving exponentials. The drawback may be overcome by Perthame's compactly supported equilibrium distribution function [11] instead of a full Maxwellian distribution. This will makes BGK scheme much simpler and attractive, which deserve further investigation.

2.3. Projection

In the projection stage, the average mass, momentum, and energy inside each cell are updated. Any inconsistent numerical treatment between the flux and the source term in this step may easily cause *numerical heating* in the simulation of gravitational gas dynamics. Here, we are going to analyze the so-called *numerical heating* reported by Slyz [13]. When *numerical heating* occurs, the computed system will continuously increase its internal energy, which is shown in Fig. 1.

Typically, there are two ways to update the energy inside each cell. One is the *non-conservative* form:

$$\frac{\partial}{\partial t}\int_\Omega E\,d\Omega + \oint_{\vec{S}}((E+p)\vec{u} - \kappa\nabla T - \overline{\overline{\Sigma}}\cdot\vec{u})\cdot d\vec{S} = \int_\Omega \rho\vec{u}\cdot(-\nabla\phi)\,d\Omega. \tag{14}$$

For a time-independent potential, the gravitational energy can be absorbed into the total energy. Therefore, the energy equation in this special case can be written in a conservative form as the following:

$$\frac{\partial}{\partial t}\int_\Omega E_{\text{tot}}\,d\Omega + \oint_{\vec{S}}((E_{\text{tot}}+p)\vec{u} - \kappa\nabla T - \overline{\overline{\Sigma}}\cdot\vec{u})\cdot d\vec{S} = 0, \tag{15}$$

where $E_{\text{tot}} = E + \rho\phi$. The discretized forms of equations (14) and (15) are

$$E_j^{n+1} = E_j^n - \frac{1}{x_{j+1/2} - x_{j-1/2}}\int_{t^n}^{t^{n+1}}(F_E(x_{j+1/2}, t) - F_E(x_{j-1/2}, t))dt + \int_{t^n}^{t^{n+1}} Q_E(x_j)dt, \tag{16}$$

$$E_{\text{tot}}^{n+1}(x_j) = E_{\text{tot}}^n(x_j) - \frac{1}{x_{j+1/2} - x_{j-1/2}}\int_{t^n}^{t^{n+1}}(F_{E_{\text{tot}}}(x_{j+1/2}, t) - F_{E_{\text{tot}}}(x_{j-1/2}, t))dt, \tag{17}$$

respectively, where the gravitational source term is

$$\int Q_E(x_j)dt = \frac{1}{\Omega}\int\int_\Omega \rho\vec{u}\cdot(-\nabla\phi)d\Omega\,dt.$$

Slyz and Prendergast concluded that Eq. (17) rather than (16) should be used to update the energy term. Otherwise, *numerical heating* will be introduced into the numerical solution because of the inaccurate computation of the source term [13]. Eventually, the numerical gravitational system will break down. This argument is perfectly correct. However, it is not totally complete. With a careful discretization of the source term in (16), we can still establish a stable and accurate solution. Numerically, the inaccuracy comes mainly from the low-order approximation and the *inconsistent* computation of the source term. Here, *inconsistency* means that the same flow variable at different locations of the governing equations are calculated by different methods. For

example, in the projection formulation, if the gravity is time-independent, then the source term in Eq. (16) can be approximated by

$$\frac{1}{\Omega} \int \int_{\Omega} \rho \vec{u} \cdot (-\nabla \phi) \mathrm{d}\Omega \, \mathrm{d}t = \frac{1}{\Omega} \int \left[\int \rho \vec{u} \, \mathrm{d}t \right] \cdot (-\nabla \phi) \mathrm{d}\Omega, \tag{18}$$

where the term in the square brackets is the time integral of the mass flux, which should be the same as the corresponding term in the continuum equation. In Slyz and Prendergast's paper [13], the mass flux in the continuous equation was calculated by an early BGK scheme (denoted as $\vec{F}_{\rho}^{\mathrm{BGK}}$), while the mass flux in Eq. (18) was computed by a bilinear interpolation (denoted as $\vec{F}_{\rho}^{\mathrm{bi}}$). Suppose their difference is $\vec{F}_{\rho}^{\mathrm{bi}} - \vec{F}_{\rho}^{\mathrm{BGK}} = \delta \vec{Q}$. If all the fluxes in (3) are calculated by the BGK method while the source term in (16) is calculated by $\vec{F}_{\rho}^{\mathrm{bi}} \cdot \frac{1}{\Omega} \int (-\nabla \phi) \mathrm{d}\Omega$, the additional source term, $\delta \vec{Q} \cdot \frac{1}{\Omega} \int (-\nabla \phi) \mathrm{d}\Omega$, will appear in the energy equation, (16). This could be the origin of *numerical heating*. Unfortunately, the error will grow in one direction in a system under gravity. The instability is closely related to the so-called *gravo-thermal instability*. But the reason is due to the numerical conservation error, instead of the physical one due to the energy loss in an astrophysical system.

For an isolated or adiabatic system, after a long time integration, any inconsistent treatment of the source term in the formulation (16) will generate *numerical heating* and the system will deviate from its physical solution. In order to avoid the instability and inaccuracy in the solution, we have taken the following two steps when using (16). The first one is to compute the source term consistently. In the current study, the mass flux at the cell interface is used to approximate the integration inside the cell. The source term, (18), is discretized as

$$\int Q_E(x_j) \mathrm{d}t = \frac{1}{2} \int (F_{\rho}^{\mathrm{BGK}}(x_{j-1/2}) + F_{\rho}^{\mathrm{BGK}}(x_{j+1/2}))(-\nabla \phi)_j \, \mathrm{d}t.$$

The second one is that the gravitational forcing effect is explicitly included in the flux evaluation as presented for the BGK scheme in the last subsection. Equipped with these two mechanisms, the scheme with (16) is still a well-balanced method up to the second-order accuracy.

When Eq. (17) is used, the time-integrated total energy flux can be written as

$$\vec{F}_{E_{\mathrm{tot}}} = \vec{F}_E + \vec{F}_{\rho} \phi.$$

Therefore, the total energy will be precisely conserved. Even through the gravitational force effect is not included in the flux evaluation in [13], based on the formulation (17) the numerical error will not grow and accumulate forever. The departure from the isothermal hydrostatic state will stay bounded due to the total energy conservation, but with large oscillations. Even when using (17), the numerical accuracy can be much improved once the gravitational force is included in the flux construction. The numerical results presented in the next section support the above argument.

3. Numerical tests and discussion

In this section, numerical tests of 1D, 2D and 3D cases are performed to validate the gas-kinetic method. Each of them is very sensitive to the accuracy of the scheme. Some of them are run for millions of numerical steps whereby the accumulation of any small error would become significant for such a long time integration.

3.1. Perturbation of the 1D isothermal equilibrium solution

This first test case is from the the paper by LeVeque and Bale [8], where a quasi-steady wave-propagation algorithm was developed for an ideal gas subject with a static gravitational field. Initially, an ideal gas with $\gamma = 1.4$ stays at an isothermal hydrostatic state,

$$\rho_0(x) = p_0(x) = \mathrm{e}^{-x}, \quad \text{and} \quad u_0(x) = 0,$$

for $x \in [0, 1]$. The gravity acts in the negative x direction, such as $-\nabla \phi(x) = -1$. Initially, the pressure is perturbed by

$$p(x, t = 0) = p_0(x) + \eta\, e^{-\alpha(x-x_0)^2},$$

where $\alpha = 100, x_0 = 0.5$, and η is the amplitude of the perturbation.

The computation is conducted with 100 grid points in the whole domain. The results from the BGK scheme with and without the gravitational source term included in the fluxes are shown in Fig. 2. The figure clearly shows that the inclusion of the source term in the flux function is very important for the accurate capturing of small perturbations. In the above calculations, the BGK scheme uses the van Leer limiter in the initial reconstruction. Therefore, the BGK scheme itself works in both the smooth and discontinuous flow regions. However, the quasi-steady wave propagation algorithm in [8] works only in the smooth flow region.

3.2. One-dimensional gas falling into a fixed external potential

This case is taken from Slyz and Prendergast's paper [13] to investigate the numerical accuracy of the BGK scheme. The gas is initially stationary ($\vec{u} = 0$) and homogenous ($\rho = 1, \epsilon = 1$, where ϵ is the internal energy). The gravitational potential has the form of a sine wave,
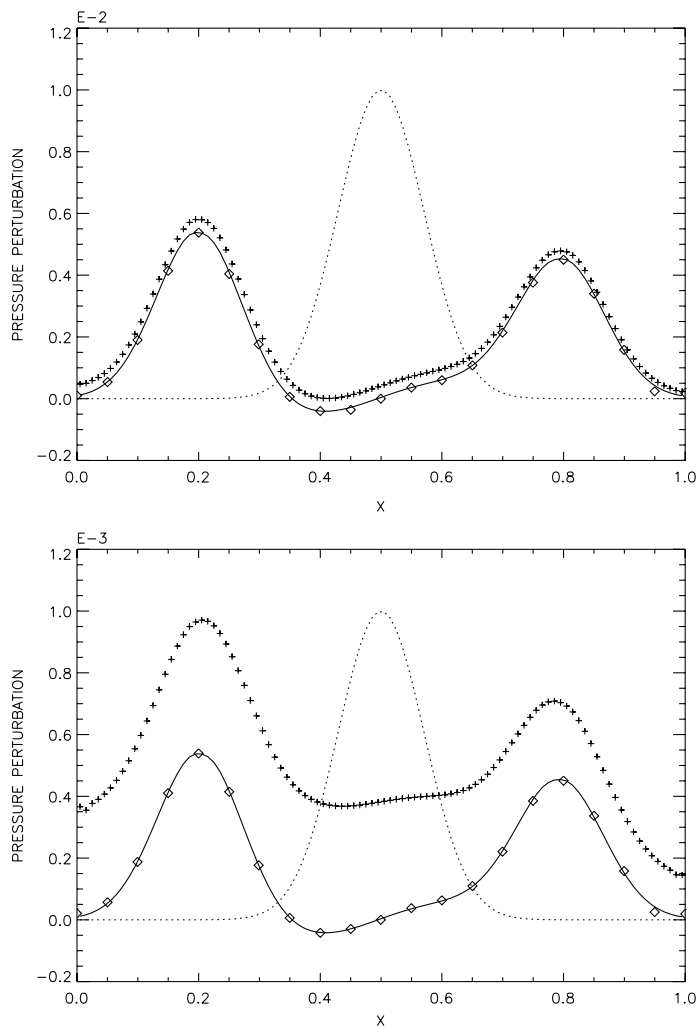
Fig. 2. Solutions of the BGK scheme with and without the source term effect in the flux function. The BGK scheme with the van Leer limiter is used in these calculations. Hundred grid points are used in the whole domain. The output time is $t = 0.25$. The upper and lower figures have the perturbations; upper: $\eta = 0.01$, lower: $\eta = 0.001$. The dotted lines show the initial pressure perturbation from a hydrostatic solution, the pluses represent the results without the source term effect in the flux, and the solid lines are the results with the source term effect. The diamonds are the reference solutions from [8].

$$\phi = -\phi_0 \frac{\mathcal{L}}{2\pi} \sin \frac{2\pi x}{\mathcal{L}},$$

where $\mathcal{L} = 64$ is the length of the computational domain and $\phi_0 = 0.02$. The ratio of the specific heat, γ, is $5/3$. The periodic boundary conditions are implemented in this system. After the initial transition, the system eventually reaches an isothermal hydrostatic distribution, where the temperature settles to a constant ($T(x,t) = T_0$) and $\vec{u} = 0$. For an ideal gas ($p = \rho RT$), from the hydrostatic equation $\partial p/\partial x = \rho(-\partial \phi/\partial x)$, the density distribution becomes $\rho(x,t) \sim \exp(-\phi/RT_0)$. However, the system is highly nonlinear since T_0 depends on ρ. It is thus better to use a numerical method to solve this problem. Each simulation result presented here is obtained with 500,000 time steps on a Cartesian grid with $\Delta x = 1$. The Courant number used is 0.9.

When the *numerical heating* occurs in an inconsistent scheme, the gas will become hotter due to the numerical error. As used by Slyz, the schemes solving Eq. (14) are named the energy source term (EST) schemes, and others solving Eq. (15) are called the energy conservation (ECT) schemes. The final state (density, velocity and temperature) of the system given in Fig. 3 is calculated from both the EST and ECT BGK schemes. A *consistent* source term treatment for the EST scheme is used, such that the mass flux integration inside each cell is approximated by the average of the cell interface mass fluxes. In the above calculation, the gravitational effect is included in the flux evaluations for both schemes. In this figure, the diamonds indicate the solutions of the ECT scheme and the solid lines indicate the solutions of the EST scheme. Fig. 3 shows that the results obtained by the EST scheme and ECT scheme are almost indistinguishable. The small derivation from the hydrostatic state in both schemes is due to the inaccurate representation of the exponential function by a single slope inside each cell. We cannot find any simple way to remedy this.

Even within the framework of the ECT scheme, in the following we are going to show that it is necessary to include the gravitational force in the flux for maintaining high accuracy. For a stationary state, $\vec{u} = 0$, it can be shown that in the current scheme the fluxes induced by the spatial derivatives $\int \vec{a} \cdot \vec{c} c_i g \vec{\psi} f \, d\Xi$ are totally balanced by the gravitational force terms $\int \vec{b} \cdot (-\nabla \phi) c_i g \vec{\psi} f \, d\Xi$, where there is no adjustable parameter. In other words, without considering the external force effect in the flux, the steady state cannot be accurately reached by a numerical scheme. The solution given in Fig. 4 is calculated by ECT scheme. The diamonds are the solution of the ECT scheme with a gravitational effect in the flux and the solid lines are the ones without the gravitational effect in the flux. Fig. 4 shows that neglect of the gravitational effect in the gas evolution stage will drive the solution away from the hydrostatic equilibrium solution even though the solution will not blow up due to the total energy conservation, the so-called ECT scheme. We believe that any scheme based on the Riemann solution, if the gravitational term is not included in the flow evolution, may have a similar problem. By including gravity, the relative fluctuation in both the velocity and temperature is much reduced. It is difficult to predict if there will be any shock capturing well-balanced scheme, where the fluid velocity in a hydrostatic equilibrium state can be kept up to the machine zero.

This test case illustrates that a simple operator splitting approach does not work and the inclusion of the gravitational force in the numerical flux is the key for a well-balanced scheme. However, it is widely recognized and proved mathematically that the Strang splitting method is a second-order accurate time-integration method for general evolutionary equations with multiple operators. In the following, we apply the Strang splitting method to this test case as well. The update of the flow variables are

$$\vec{U}^{n+1} = S[\Delta t/2] H_{\text{BGK}}[\Delta t] S[\Delta t/2] \vec{U}^n, \tag{19}$$

where S represents the source term contribution inside each cell, and H_{BGK} is the BGK flux across a cell interface without including the gravitational force term. The results from the EST BGK scheme and the above EST Strang splitting method are shown in Fig. 5. The Strang splitting method gives accurate velocity solution, which is similar to that from EST BGK. However, the temperature of the EST Strang solution is continuously increasing with the total number of integration steps. For a slow gas evolution system under gravitational field, the numerical heating from the Strang splitting method will become severe.

3.3. Onset of two-dimensional compressible convection

Consider a fluid confined by two horizontal parallel plates, where the gravity is imposed vertically, and the upper plate is fixed at a lower temperature while the lower plate is fixed at a higher temperature. For inviscid
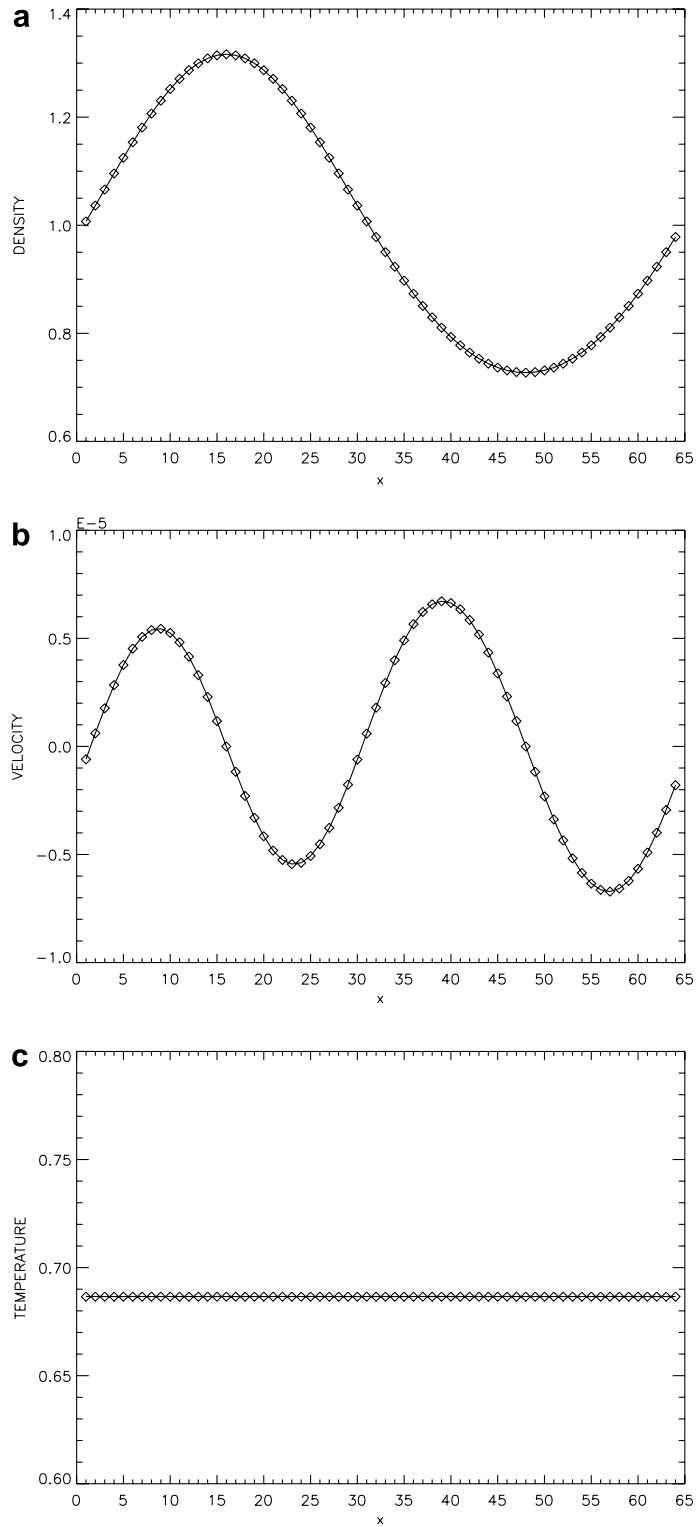
Fig. 3. Comparison of the EST (diamonds) and ECT (solid lines) schemes. These results were obtained after 500,000 time steps.
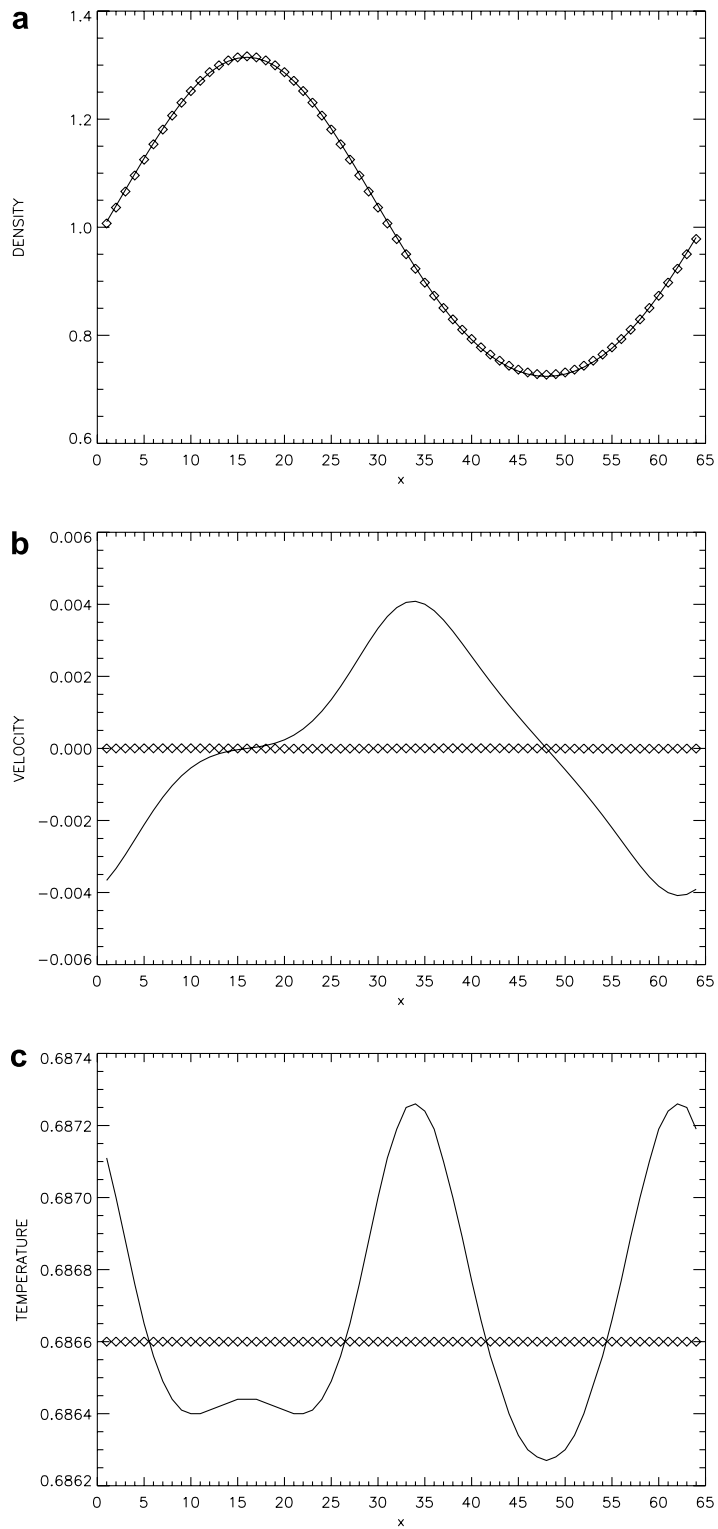
Fig. 4. Results of the ECT scheme with the external force term in the flux (diamonds), and the ECT scheme without including external force term in the flux (solid lines). These results were obtained after 500, 000 time steps.
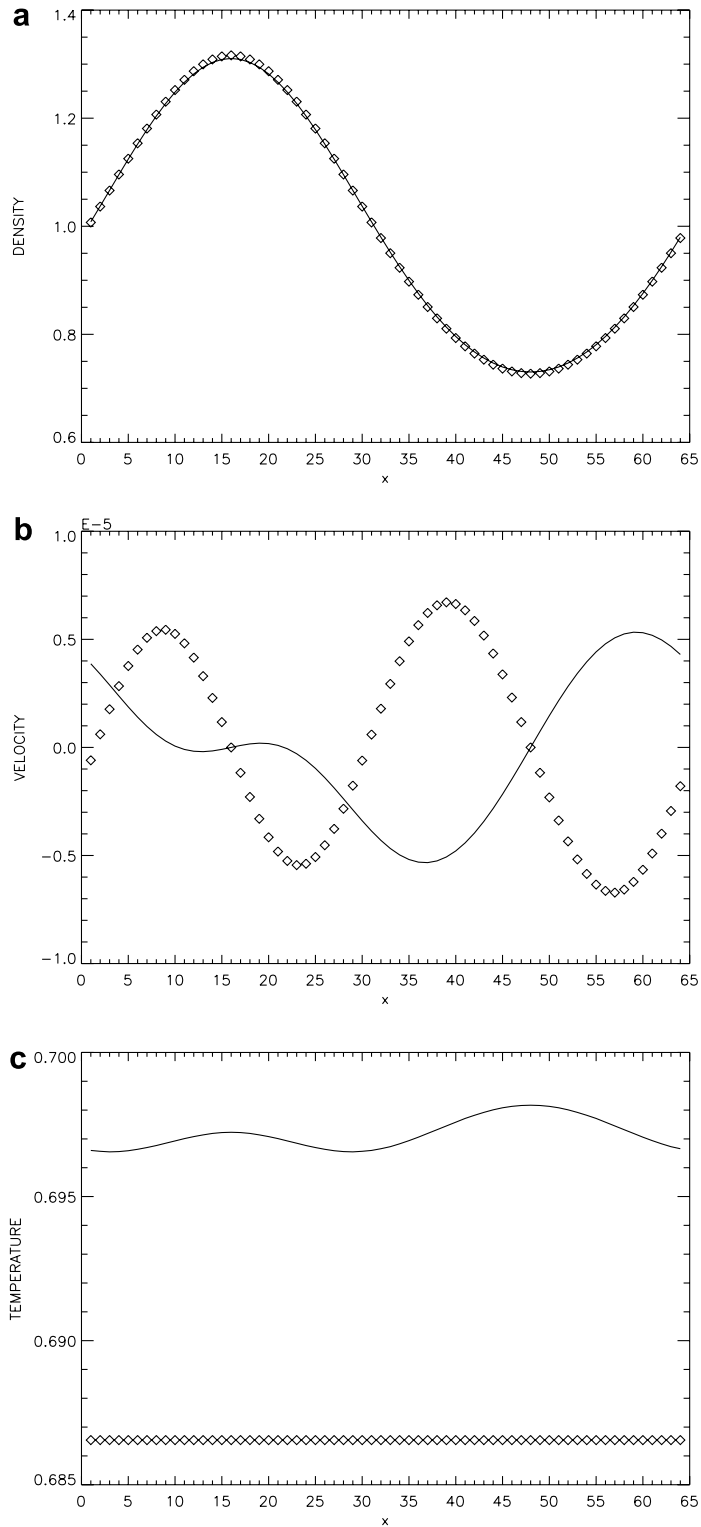
Fig. 5. Results of the current EST BGK scheme (diamonds) and the Strang splitting method (solid lines). The results were obtained after 500,000 time steps.

fluids, when the temperature gradient exceeds the adiabatic temperature gradient, the system becomes convectively unstable. In the astrophysics literature, such a condition is known as the Schwarzschild criterion for convection ([7, p. 39]). For general cases where the viscosity is taken into account, the motion is always impeded by the viscosity, and the temperature gradient is reduced by the thermal conductivity. To study the general situation, the Rayleigh number is used to indicate the combined effects of the dynamical viscosity, thermal diffusion and temperature gradient. The steady convection will not occur unless the Rayleigh number is larger than a specific value, i.e., the critical Rayleigh number. The compressible convection is a sensitive test on the accuracy and stability of any numerical scheme. The onset of stable large-scale circulation depends sensitively on the numerical dissipation and boundary treatment. A low-order scheme may introduce too much artificial dissipation, which increases the critical Rayleigh number. Due to the large scale in height and pressure changes, the instability can be triggered easily.

In the gas-kinetic BGK scheme, the dissipative coefficient is controlled by the particle collision time. In a continuous flow region, only physical viscosity needs to be used. However, there are two ways to add the artificial dissipation in a numerical scheme to enhance the shock capturing ability. The *kinematic* dissipation can be introduced through limited reconstructed initial data, which implicitly transfers kinetic energy into thermal energy. The *dynamical* dissipation can be added as well by enlarging the viscosity coefficient in the governing equations according to the pressure jump at the cell interface [15]. Note that any discontinuity in the reconstructed data means the cell resolution is not enough to resolve the flow structure. Here, the evaluation of the critical Rayleigh numbers for the two-dimensional compressible convection case is a good indication of the accuracy and robustness of the scheme.

In this section, we adopt the cases calculated by Grahma [6] and Chan [3] for the purpose of comparison. Consider an ideal gas confined in a box with $0 \leqslant x_1 \leqslant l, 0 \leqslant x_2 \leqslant d$. The free surface and isothermal boundary conditions are imposed at the top and bottom boundaries,

$$u_2 = 0, \quad \frac{\mathrm{d}u_1}{\mathrm{d}x_2} = 0, \quad T = T_\mathrm{b}, T_t, \quad \text{at } x_2 = 0, d,$$

and the stress-free insulated boundary conditions are imposed in the horizontal direction,

$$u_1 = 0, \quad \frac{\mathrm{d}u_2}{\mathrm{d}x_1} = 0, \quad \frac{\mathrm{d}T}{\mathrm{d}x_1} = 0, \quad \text{at } x_1 = 0, l.$$

The initial condition is the static state with a small perturbation in the velocity field,

$$T = (1 + Z(d - x_2)/d)T_t,$$
$$\rho = (T/T_t)^m \rho_t,$$
$$p = (T/T_t)^{m+1} p_t,$$

where $Z = (T_\mathrm{b} - T_t)/T_t$ is the normalized parameter, and m is the polytropic gas index. There is a hydrostatic solution of the Navier–Stokes equations with a uniform constant gravitational acceleration,

$$-\nabla \phi = -\frac{(m + 1)ZRT_t}{d}.$$

With the above T, ρ, and p distributions, the initial vertical velocity is perturbed by

$$u_1 = 0,$$
$$u_2 = u_0 \sin\frac{2\pi x_1}{l} \sin\frac{\pi x_2}{d},$$

where u_0 is a very small constant. Actually, the initial perturbation for the vertical velocity may be randomly generated with the satisfaction of the boundary condition. The above form leads to a faster startup of the convective rolls. All the quantities, ρ_t, p_t, T_t, d and l, are normalized. In all computations presented here, $\gamma = 5/3$, $Pr = 1$ and $m = 1.4$ are used. The Rayleigh number is defined as

$$Ra = \frac{PrRT_t Z^2 d^2 \rho_t^2}{\mu^2} \left[\frac{1 - (\gamma - 1)m}{\gamma} \right] (m + 1). \tag{20}$$

The standard solutions of the two dimensional laminar convection are shown in Fig. 6. A discussion of these solutions can be found in [4].

For each Z, the calculation is repeated with two slightly supercritical Rayleigh numbers, Ra_1 and Ra_2. Then, the critical Rayleigh number is determined by fitting the curve $\max(u_2) = A\exp(B(Ra - Ra_c)t)$ by a least square approximation, where u_2 is the vertical velocity, Ra_c is the critical Rayleigh number, and A and B are the constants to be determined. The results given in Table 1 are obtained from the current BGK scheme, where a continuous interpolation (4) is used in the reconstruction stage. From Table 1, we can see that the current BGK scheme is an accurate method for a viscous flow under a gravitational field. The difference between the critical Rayleigh numbers calculated from the gas-kinetic BGK scheme and those from the linear analysis is less than 3.5% for $Z \leqslant 10$ and $\leqslant 1\%$ for $Z < 4$. Also, the Courant number used for each calculation is included in Table 1. When a nonlinear limiter, Eqs. (5) and (6), is used in the reconstruction of the initial data, discontinuities at the cell interfaces will be introduced. This will generate extra *kinematic* dissipation. Certainly, the interface discontinuity will become smaller for higher-order interpolation in the smooth region, as will the numerical dissipation. But, instead of using higher-order interpolation, the van Leer limiter is always used in this paper because of its robustness and simplicity. To investigate the effect of the limiter on the Rayleigh number, the gas-kinetic BGK scheme with the van Leer limiter is used for the same calculation. The numerical computation shows that, for the weakly compressible flow, the critical Rayleigh number
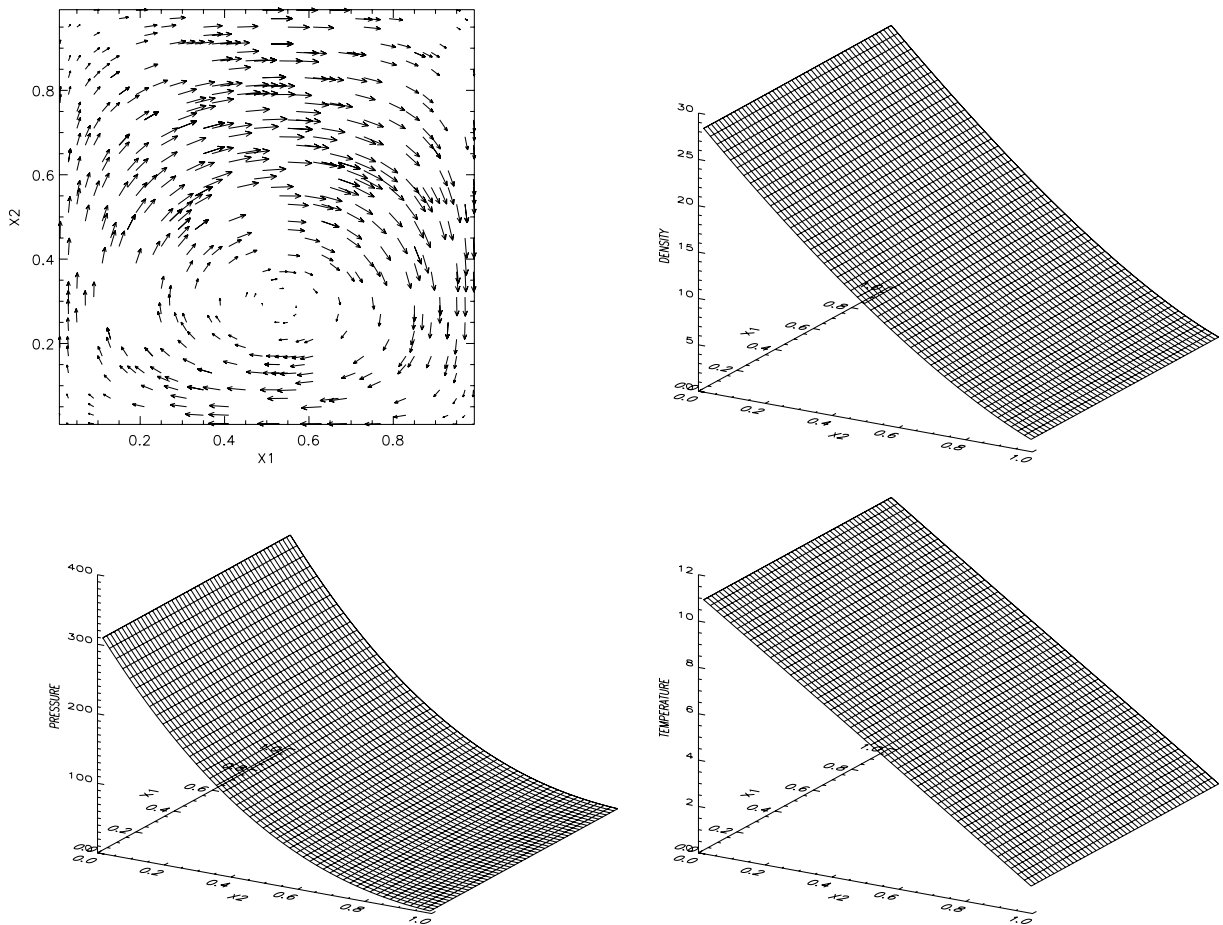

Fig. 6. Solutions of two-dimensional laminar convection obtained by the BGK scheme. The upper-left, upper-right, lower-left and lower-right plots show the velocity vector field, the density distribution, the pressure distribution, and temperature distribution, respectively. The corresponding parameters are $Z = 10$ and $Ra = 61$.

Table 1
Critical Rayleigh number

Z	0.5	1	2	4	10
Ra^a	545.03	422.79	288.51	164.88	58.17
Ra^b	550.02	424.84	289.82	167.24	59.96
δ^c	0.4	0.2	0.1	0.07	0.02

[a] Linear analysis results from Graham [6].
[b] Results from current gas-kinetic BGK scheme.
[c] Courant number.

becomes slightly larger ($Ra = 553.67$ for $Z = 0.5$), while for highly compressible flow, the situation is complex. The critical Rayleigh number becomes a little bit smaller ($Ra = 289.51$) for $Z = 2$ and larger ($Ra = 167.5$) for $Z = 4$. For $Z = 10$, the instability appears near the upper surface. This can be explained by the use of a limiter, which continuously perturbs the boundary layer through the introduction of numerical discontinuities. The limiter generates a jump in the vertical velocity field. A direct remedy for this is to use the high-resolution interpolation, or modify the initial dissipative terms in f_0 to make these terms continuous across the cell interface [10]. However, this error due to the limiter could be ignored for small and modest Z. In conclusion, a nonlinear limiter will introduce numerical dissipation, but its effect on the calculation of the critical Rayleigh number is tolerable. Furthermore, for $Pr \ll 1$ cases, the effect from the nonlinear limiter becomes negligible, where the heat conduction dominates and smoothes the flow field.

3.4. Thermodynamic properties of the laminar convection in 3D

In the numerical flux, the derivatives of the flow distribution in the tangential direction of a cell interface are taken into account in the current scheme. The current scheme is essentially a multidimensional method, where the physical effect from both gradients in the normal and tangential directions is taken into account. In order to verify the necessity of this kind of discretization, tests of compressible convection in a three-dimensional box will be presented in this subsection.

The two-dimensional model in the previous subsection is extended to three dimensions. The aspect ratio of the rectangular box is 1:0.1:1. The insulated solid well boundary conditions are applied in the horizontal directions (x_1 and x_2). Initially, the velocity field is perturbed in all directions: x_1, x_2 and x_3. The Courant number takes a value of 0.3 and the grid size is $50 \times 5 \times 50$. Unless otherwise specified, all the parameters in this subsection have the same value as those in the previous subsection.

Among the solutions, the maximum Mach number and Nusselt number are used to measure the thermodynamical property and convective heat transfer. The maximum Mach number is defined as

$$Mc = \max \left\{ \frac{|u|}{\sqrt{\gamma RT}} \right\},$$

which sensitively depends on the viscosity. The Nusselt number is used to compare the flux carried by the heat conduction and by convection. Following Graham [6], it is defined as,

$$Nu = \frac{F_t - F_a}{F_c - F_a},$$

where $F_a = -\Delta \phi k / c_p$, $F_c = \kappa (T_b - T_t)/d$ are the heat flux due to the adiabatic gradient and conduction, respectively. Let

$$F_t = \overline{\rho c_p T u_3 + \kappa \frac{dT}{dx_3}}$$

be the total heat flux, where the over-bar means the average over the whole computational domain. Numerical experiments show that Nu cannot be correctly obtained with a low-order scheme. We also introduce the relative Rayleigh number:

$$R^* = \frac{R}{Rc},$$

where R is defined by Eq. (20) and Rc is the critical Rayleigh number from the linear analysis.

A series of finite amplitude steady solutions is calculated with different Rayleigh numbers. The depth parameter is fixed to a unit. The results of one-cell circulation are given in Tables 2 and 3. The comparison with Graham's results is shown in Fig. 7.

From plot (a) in Fig. 7 we can see that the agreement is good when the central interpolation is used for the initial reconstruction (the average deviation $\bar{\sigma} \leqslant 9\%$). The agreement is better for larger Rayleigh numbers, for example, $\sigma(R^* = 100) \leqslant 5\%$. This is expected since a BGK scheme with a central interpolation is similar to the Lax–Wendroff scheme, which was used by Graham [6]. As pointed out in the previous section, the numerical dissipation will be introduced when the van Leer limiter is adopted. The average deviation of the results with different reconstructions is less than 2%. This kind of discrepancy increases with the Rayleigh number ($\sigma(R^* = 3) = 1.4\%$ and $\sigma(R^* = 100) = 3.4\%$).

The trend of the discrepancy in plot (b) of Fig. 7 is similar to that in plot (a), except that the best fitting results come with the van Leer limiter. The average deviations from Graham's results are approximately less than 3% and 5% using the van Leer limiter and the central interpolation, respectively. The Nusselt numbers obtained from the BGK scheme are systematically larger than Graham's results.

The effects of including tangential derivatives, i.e., the so-called multidimensionality, into the numerical fluxes have been checked. The results obtained from a dimensional-splitting BGK method,

$$\vec{U}_*^{n+1} = H_{x_1}\vec{U}^n,$$
$$\vec{U}_{**}^{n+1} = H_{x_2}\vec{U}_*^{n+1},$$
$$\vec{U}^{n+1} = H_{x_3}\vec{U}_{**}^{n+1} + \vec{Q}(\vec{U}_{**}^{n+1}),$$

are also listed in Tables 2 and 3, where H_{x_i} is the one-dimensional operator and $\vec{Q}$ is the source term. In the computation of the numerical fluxes, the tangential derivatives are excluded. In the directional splitting method, it is clear that additional numerical dissipation is added to the scheme because the maximum Mach numbers in the third row of Table 2 are systematically less than those in the second row. The situation is

Table 2
Maximum Mach number (Mc) vs. relative Rayleigh Number (R^a)

R^a	3	7	10	30	70	100
Mc^b	0.072	0.097	0.107	0.136	0.161	0.172
Mc^c	0.071	0.096	0.106	0.134	0.156	0.166
Mc^d	0.067	0.095	0.104	0.131	0.151	0.159[a]

[a] Temporally averaged value.
[b] Current BGK scheme with central interpolation.
[c] Current BGK scheme with the van Leer limiter interpolation.
[d] Dimensional-splitting BGK scheme with the van Leer limiter.

Table 3
Nusselt number (Nu) vs. relative Rayleigh Number (R^d)

R^d	3	7	10	30	70	100
Nu^a	2.575	3.729	4.334	6.938	10.000	11.676
Nu^b	2.533	3.702	4.299	6.831	9.675	11.141
Nu^c	2.236	3.393	3.989	6.777	9.849[d]	11.252[d]

[a] Current BGK scheme with central interpolation.
[b] Current BGK scheme with the van Leer limiter.
[c] Dimensional-splitting BGK scheme with the van Leer limiter.
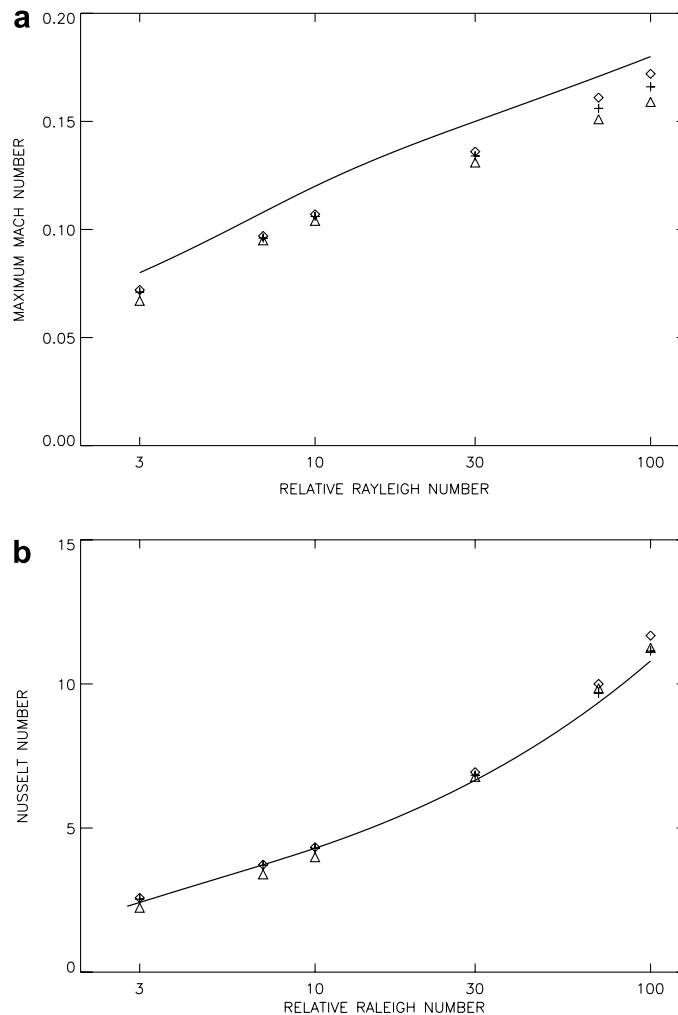[d] Temporally averaged values.

Fig. 7. Maximum Mach number (a) and Nusselt number (b) vs. relative Rayleigh numbers. The solid lines are the results from Graham's paper [6] and the diamonds and pluses represent the results computed by the BGK schemes with central interpolation and the van Leer limiter reconstruction. The triangles show the results from the dimensional-splitting BGK scheme with the van Leer limiter.

complicated for the Nusselt number. When a dimensional-splitting method is used, the convection becomes slightly turbulent for $R^* \geqslant 70$. The numbers with a superscript $*$ represent temporally averaged values. The standard deviation for $Mc(R^* = 100)$, $N(R^* = 70)$ and $N(R^* = 100)$ are 0.001, 0.003 and 0.226, respectively. When the flow becomes turbulent, the Nusselt numbers from the multidimensional scheme are a bit smaller than those from the dimensional-splitting scheme which indicates that the turbulence has a more efficient way to transfer the heat than the laminar flow. This test clearly shows that the multidimensional scheme is more stable and accurate than the dimensional-splitting scheme. The reason lies in the fact that to keep both normal and tangential derivatives in the evaluation of a flux function in a circulation motion is close to the physical reality.

3.5. Rayleigh–Taylor instability

This test case is similar to LeVeque and Bale's Rayleigh–Taylor instability case [8], which was used to validate their quasi-steady wave propagation scheme. Consider an isothermal equilibrium ideal gas ($\gamma = 1.4$) in a 2D polar coordinate,
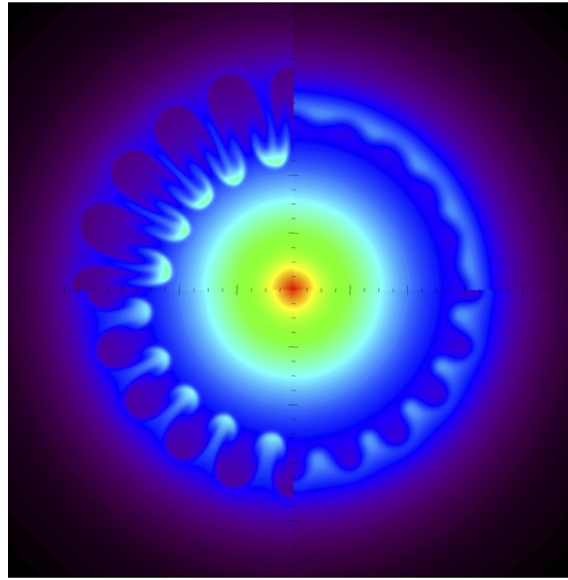
Fig. 8. A Rayleigh–Taylor instability with gravitational field directed radially inward. Density contours at four different times ($t = 0.0, 0.8, 1.4$, and 2.0) are shown in the four quadrants, starting with the initial data in the upper right corner and progressing clockwise.

$$\rho_0(r) = e^{-\alpha(r+r_0)},$$
$$p_0(r) = \frac{1.5}{\alpha} e^{-\alpha(r+r_0)},$$
$$-\nabla\phi(r) = -1.5,$$
$$u_0 = 0,$$

where $\alpha = 2.68, r_0 = 0.258$ for $r \leqslant r_1$ and $\alpha = 5.53, r_0 = -0.308$ for $r > r_1$ with

$$r_1 = 0.6(1 + 0.02\cos(20\theta))$$

for density and

$$r_1 = 0.62324965$$

for pressure. In this case, two different isothermal equilibrium states intersect around $r = 0.6$ with density and pressure perturbations.

Due to the geometric symmetry in this problem, only the solution in the first quadrant is computed. The computational domain, $[0,1] \times [0,1]$, is covered by 120×120 uniform grid points. The CFL number takes a value 0.6. On the axis of symmetry, a rotated periodic boundary condition is used. At the other boundaries, the values in the ghost cells are fixed as their initial values in order to keep the isothermal equilibrium solution there. Fig. 8 presents the time evolutions of the density distributions at times $t = 0.0, 0.8, 1.4$, and 2.0. Fig. 9 shows a scatter plot of the density as a function of the radius. Note that, away from the location ($r \simeq r_0$), the current method retains the hydrostatic equilibrium solution and radial symmetry very well.

4. Conclusions

The gas-kinetic BGK scheme for the Navier–Stokes equations is extended to include external gravitational forces. Our study allows us to draw the following conclusions. (1) The gravitational force effect should be included in the evaluation of the numerical fluxes across a cell interface. It has the first-order effect in time [16], which cannot be neglected in a second-order scheme. In a gas-kinetic scheme, the external force modifies the time evolution of both the initial gas distribution function and the local equilibrium state through the par-
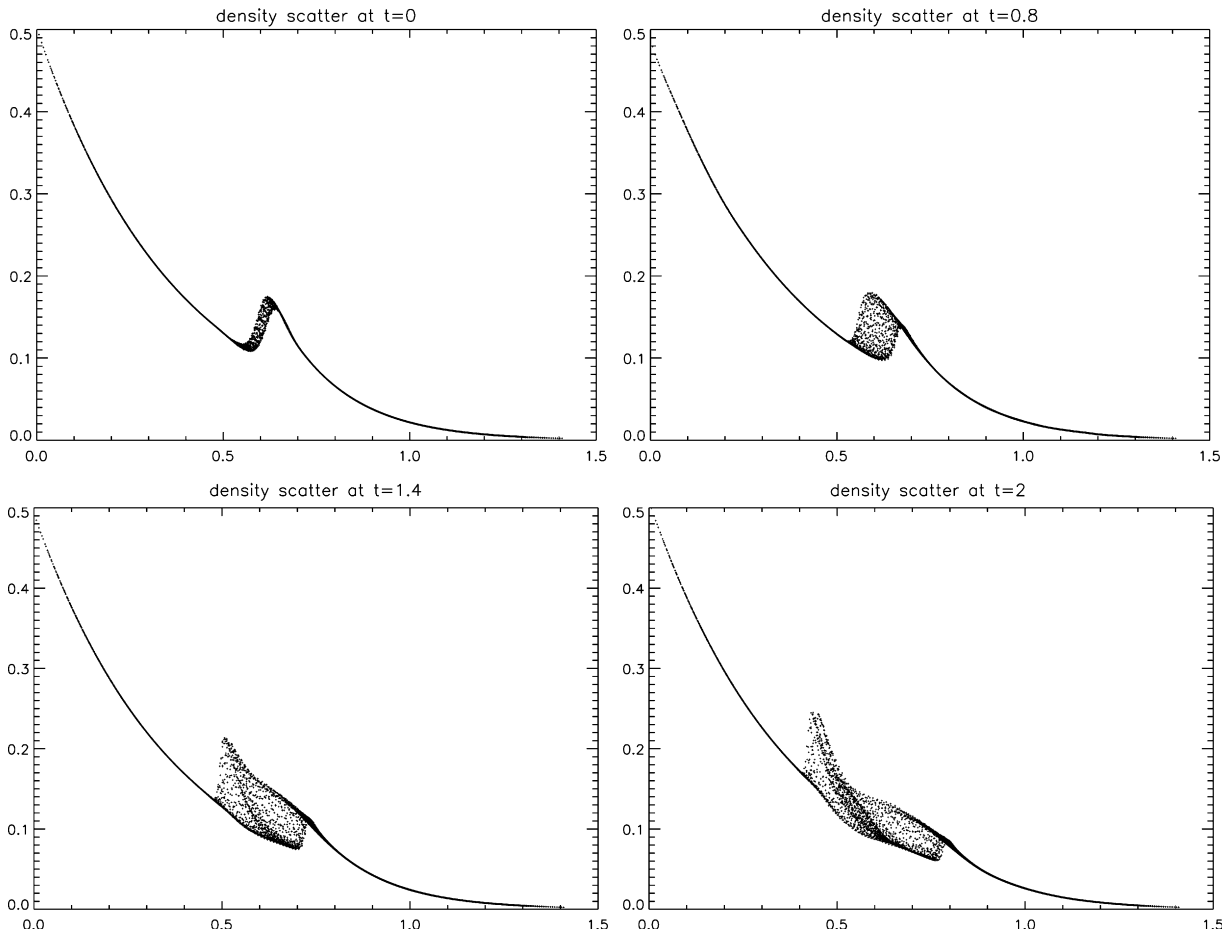
Fig. 9. Scatter plots of the density in the cell vs. the distance of the cell center from the origin. The density is shown at four different times ($t = 0.0, 0.8, 1.4,$ and 2.0). The single line away from r_0 indicates the capacity of the current scheme to keep the hydrostatic equilibrium solution.

ticle acceleration. Without such an implementation, it is impossible for the system to settle down to a highly accurate hydrostatic equilibrium state. (2) Numerical heating is mainly caused by the inconsistent treatment of the gravitational source terms inside each cell in the energy source term scheme. After a long time evolution, the numerical error will accumulate and dramatically affect the final solution of an isolated or insulated gravitational system. For a system that exchanges energy with its surrounding environment or that has a short evolution time, such as the star explosion case, this kind of numerical heating may not appear to be significant. (3) The numerical simulation of the onset of two-dimensional laminar convection shows that the current BGK scheme can accurately determine the critical Rayleigh numbers. However, the nonlinear limiter is usually harmful to the smooth flow solution. High-order interpolation may alleviate this problem. (4) The results of finite amplitude laminar convection with a central interpolation agree well with Graham's results. The van Leer limiter introduces a bit of additional dissipation. By including the tangential gradient terms, i.e., the so-called multidimensional approach, the accuracy of the scheme is improved. The kinetic scheme presented in this paper is not solely limited to hydrodynamics under gravitational fields; it can be applied to other systems in which the external force term can be an electric field force, such as the Boltzmann-type equations for semi-conductor devices.

Developing a well-balanced scheme for gas dynamic equations under gravitational fields is still an open problem. It is much more difficult than developing a scheme for the shallow water equations. We hope that this paper will help to shift attention from shallow water equations to gas dynamic equations. At the current

stage, it seems that no currently available scheme can maintain the velocity of the hydrostatic equilibrium state up to the machine zero, such as on the order of 10^{-16}. At the same time, the scheme has a shock capturing ability. Even with consideration of all the techniques presented in this paper, the current method has only second-order accuracy in maintaining the hydrostatic solution. Much work is left for the future.

Acknowledgments

Appendix. Solution of matrix equation $b = \mathbf{M}a$ in the three-dimensional case

In the gas-kinetic scheme, to obtain the derivatives of a Maxwellian, the solution of the following equations need to be evaluated,

$$
\begin{pmatrix} b_1 \\ b_2 \\ b_3 \\ b_4 \\ b_5 \end{pmatrix} = \mathbf{M} \begin{pmatrix} a_1 \\ a_2 \\ a_3 \\ a_4 \\ a_5 \end{pmatrix}, \tag{21}
$$

where b and $\mathbf{M}$ are known. The matrix $\mathbf{M}$ is defined as

$$
\mathbf{M} = \frac{1}{\rho} \int \vec{\psi} \otimes \vec{\psi} f^{\mathrm{eq}} \, \mathrm{d}\varXi,
$$

where f^{eq} is the Maxwellian.

The details of the matrix $\mathbf{M}$ are given by

$$
\mathbf{M} = \begin{pmatrix}
1 & u_1 & u_2 & u_3 & B_1 \\
u_1 & u_1^2 + 1/2\lambda & u_1 u_2 & u_1 u_3 & B_2 \\
u_2 & u_1 u_2 & u_2^2 + 1/2\lambda & u_2 u_3 & B_3 \\
u_3 & u_1 u_3 & u_2 u_3 & u_3^2 + 1/2\lambda & B_4 \\
B_1 & B_2 & B_3 & B_4 & B_5
\end{pmatrix},
$$

where

$$
B_1 = \frac{1}{2} \left(u_1^2 + u_2^2 + u_3^2 + (K+3)/2\lambda \right),
$$

$$
B_2 = \frac{1}{2} \left(u_1^3 + u_1(u_2^2 + u_3^2) + (K+5)u_1/2\lambda \right),
$$

$$
B_3 = \frac{1}{2} \left(u_2^3 + u_2(u_1^2 + u_3^2) + (K+5)u_2/2\lambda \right),
$$

$$
B_4 = \frac{1}{2} \left(u_3^3 + u_3(u_1^2 + u_2^2) + (K+5)u_3/2\lambda \right),
$$

and

$$
B_5 = \frac{1}{4} \left((u_1^2 + u_2^2 + u_3^2)^2 + (K+5)(u_1^2 + u_2^2 + u_3^2)/\lambda + (K+3)(K+5)/4\lambda^2 \right).
$$

Defining

$$R_5 = 2b_5 - \left(u_1^2 + u_2^2 + u_3^2 + \frac{K+3}{2\lambda}\right)b_1,$$

$$R_4 = b_4 - u_3 b_1,$$

$$R_3 = b_3 - u_2 b_1,$$

$$R_2 = b_2 - u_1 b_1,$$

the solutions of Eq. (21) are

$$a_5 = \frac{4\lambda^2}{K+3}(R_5 - 2u_1 R_2 - 2u_2 R_3 - 2u_3 R_4),$$

$$a_4 = 2\lambda R_4 - u_3 a_5,$$

$$a_3 = 2\lambda R_3 - u_2 a_5,$$

$$a_2 = 2\lambda R_2 - u_1 a_5,$$

and

$$a_1 = b_1 - u_1 a_2 - u_2 a_3 - u_3 a_4 - \frac{1}{2}a_5\left(u_1^2 + u_2^2 + u_3^2 + \frac{K+3}{2\lambda}\right).$$

References

[1] P.L. Bhatnagar, E.P. Gross, M. Krook, A model for collision processes in gases I: small amplitude processes in charged and neutral one-component systems, Phys. Rev. 94 (1954) 511–525.
[2] N. Botta, R. Klein, S. Langenberg, S. Lutzenkirchen, Well-balanced finite volume methods for nearly hydrostatic flows, J. Comput. Phys. 196 (2004) 539–565.
[3] K.L. Chan, C.L. Wolff, ADI on staggered mesh – a method for the calculation of compressible convection, J. Comput. Phys. 47 (1982) 109–129.
[4] S. Chandrasekhar, Hydrodynamic and Hydromagnetic Stability, Oxford University Press, 1961.
[5] C.S. Frenk et al., The Santa Barbara cluster comparison project: a comparison of cosmological hydrodynamics solutions, The Astrophy. J 525 (1999) 554–582.
[6] E. Graham, Numerical simulation of two-dimensional compressible convection, J. Fluid. Mech. 70 (1975) 689–703.
[7] R. Kippenhahn, A. Weigert, Stellar Structure and Evolution, Springer-Verlag, Berlin, 1990.
[8] R.J. LeVeque, D.S. Bale, Wave propagation methods for conservation laws with source terms, in: Proceedings of the 7th International Conference on Hyperbolic Problems, Zurich, February, 1998.
[9] Q. Li, S. Fu, On the multidimensional gas-kinetic BGK scheme, J. Comput. Phys. 220 (2006) 532–548.
[10] G. May, B. Srinivasan, A. Jameson, An improved gas-kinetic BGK finite-volume method for three-dimensional transonic flow, J. Comput. Phys. 220 (2007) 856–878.
[11] B. Perthame, Boltzmann type schemes for gas dynamics and the entropy property, SIAM J. Numer. Anal. 27 (6) (1990) 1405–1421.
[12] D. Ryu, J.P. Ostriker, H. Kang, R. Cen, A cosmological hydrodynamic code based on the total variation diminishing scheme, Astrophy. J. 414 (1993) 1–19.
[13] A. Slyz, K.H. Prendergast, Time-independent gravitational fields in the BGK scheme for hydrodynamics, Astron. Astrophys. Suppl. Ser. 139 (1999) 199–217.
[14] M. Sun, T. Saito, P.A. Jacobs, et al., Axisymmetric shock wave interaction with a cone: a benchmark test, Shock Waves 14 (2005) 313–331.
[15] K. Xu, A gas-kinetic BGK scheme for the Navier–Stokes equations and its connection with artificial dissipation and Godunov method, J. Comput. Phys. 171 (2001) 289–335.
[16] K. Xu, A well-balanced gas-kinetic scheme for the shallow-water equations with source terms, J. Comput. Phys. 178 (2002) 533–562.
[17] K. Xu, E. Josyula, Continuum formulation for non-equilibrium shock structure calculation, Commun. Comput. Phys. 1 (2006) 425–450.
[18] E.F. Toro, Riemann Solvers and Numerical Methods for Fluid Dynamics, Springer, New York, 1999.
[19] W.G. Vincent, C.H. Kruger Jr., Introduction to Physical Gas Dynamics, Wiley, New York, 1965.
[20] M. Zingale et al., Mapping initial hydrostatic models in Godunov codes, Astro. Phys. J. Suppl. 143 (2002) 539–565.